PAPER

On the mechanisms governing gas penetration into a tokamak plasma during a massive gas injection

To cite this article: E. Nardon *et al* 2017 *Nucl. Fusion* **57** 016027

IOP Publishing | International Atomic Energy Agency Nuclear Fusion

Nucl. Fusion **57** (2017) 016027 (13pp) doi:10.1088/0029-5515/57/1/016027

On the mechanisms governing gas penetration into a tokamak plasma during a massive gas injection

E. Nardon[1], A. Fil[1,a], P. Chauveau[1,b], P. Tamain[1], R. Guirlet[1], H.R. Koslowski[2], M. Lehnen[3], C. Reux[1], F. Saint-Laurent[1] and JET Contributors[4,c]

[1] CEA, IRFM, F-13108 Saint-Paul-lez-Durance, France
[2] Forschungszentrum Jülich GmbH, Institut für Energie und Klimaforschung—Plasmaphysik, 52425 Jülich, Germany
[3] ITER Organization, Route de Vinon sur Verdon, 13115 Saint Paul Lez Durance, France
[4] EUROfusion Consortium, JET, Culham Science Centre, Abingdon, OX14 3DB, UK

E-mail: eric.nardon@cea.fr

Received 22 March 2016, revised 27 September 2016
Accepted for publication 30 September 2016
Published 15 November 2016

Abstract

A new 1D radial fluid code, IMAGINE, is used to simulate the penetration of gas into a tokamak plasma during a massive gas injection (MGI). The main result is that the gas is in general strongly braked as it reaches the plasma, due to mechanisms related to charge exchange and (to a smaller extent) recombination. As a result, only a fraction of the gas penetrates into the plasma. Also, a shock wave is created in the gas which propagates away from the plasma, braking and compressing the incoming gas. Simulation results are quantitatively consistent, at least in terms of orders of magnitude, with experimental data for a D_2 MGI into a JET Ohmic plasma. Simulations of MGI into the background plasma surrounding a runaway electron beam show that if the background electron density is too high, the gas may not penetrate, suggesting a possible explanation for the recent results of Reux *et al* in JET (2015 *Nucl. Fusion* **55** 093013).

Keywords: disruption mitigation, massive gas injection, fluid dynamics

(Some figures may appear in colour only in the online journal)

1. Introduction

Due to the potentially deleterious consequences of disruptions in ITER, a disruption mitigation system (DMS) is needed [2, 3]. Its design, which is presently underway, is based on the use of massive material injection, in the form of either gas (massive gas injection or MGI) or shattered pellets [4, 5]. This paper focuses on MGI and more specifically on its modelling. Our objective is to identify key mechanisms which determine the penetration of the gas into the plasma and to study their dependency on plasma parameters.

MGI consists in releasing a large amount of gas (compared to the plasma content) by suddenly opening a gas reservoir, which can be located from a few cm to a few m away from the plasma. After a certain time of propagation in vacuum, the arrival of the gas into the plasma typically leads to an increase of the electron density n_e and the propagation of a cold and radiating front into the plasma (see for example figure 12 in [6] for high-resolution profiles in MAST). At some point, a thermal quench (TQ) is triggered. There is evidence in several

[a] Present address: Princeton University, NJ 08540, USA
[b] Present address: GANIL, CEA/DSM CNRS/IN2P3, Bvd Henri Becquerel, 14076 Caen, France
[c] See the appendix of Romanelli *et al* [34]

machines (e.g. MAST [6], Tore Supra [8] and TEXTOR [7]) that the TQ is triggered when the cold front reaches the $q = 2$ surface.

Significant work has been devoted by experimentalists to the estimation of the ratio between the increase in the number of electrons ΔN_e and the number of gas atoms that have reached the edge of the plasma, $N_{\rm inj}$ (the latter being estimated using models for the gas propagation into vacuum) [8–11]. This ratio, which is often called 'fuelling efficiency' and noted $F_{\rm eff}$, is indeed of importance regarding, for example, the objective of suppressing runaway electrons (RE) by increasing $n_{\rm e}$ [4, 5]. Depending on the type of gas, the reservoir pressure and characteristics (e.g. its distance to the plasma) and the plasma parameters, $F_{\rm eff}$ can vary significantly, typically from a few percent to a few tens of percent. This indicates that the gas penetrates only partially, and sometimes even marginally, into the plasma. This is consistent with, for example, the observation from DIII-D that 'over a wide range of initial target conditions [...], visible camera images of neutral Ar emission indicate that the propagation of jet neutrals is stopped at the plasma edge ($\simeq$ 0–5 cm past the separatrix) during the TQ' [12]. Another important recent result possibly related to the question of gas penetration is the unsuccessful attempt to suppress an RE beam after its formation using MGI on JET [1]. One possible reason for this failure is indeed that the gas does not penetrate deep enough into the background plasma and thus cannot reach the RE beam. Clearly, the above points motivate efforts to understand the mechanisms governing gas penetration during an MGI. The development of a new 1D radial fluid code called IMAGINE and its application to MGI simulations described below are part of these efforts.

A number of codes have been used for MGI modelling in the past, including ASTRA [13, 14], TOKES [15, 16], SOLPS [17], NIMROD [18–22], JOREK [23, 35] and the code of Rozhansky *et al* [24]. Compared to these works, the approach presented here is original in that it treats gas transport as purely convective (as it should be, according to first principles) and it includes the gas reservoir, vacuum region and plasma in the simulation domain. These ingredients are essential to simulate the processes described below.

The paper is constructed as follows. Section 2 presents the model and the IMAGINE code. Section 3 describes simulations of a D_2 MGI into a JET Ohmic plasma, discusses the mechanisms at play and compares the results to experimental observations. Section 4 presents simulations whose aim is to investigate the penetration of the gas into the background plasma co-existing with a RE beam. Section 5 then comes back to the justifiability and limits of the IMAGINE model. Finally, section 6 concludes and gives perspectives.

2. Model

2.1. Geometry, equations and assumptions

The model is 1D in the radial direction and assumes a slab geometry (for readability purposes, we have chosen to defer the discussion of the justifiability and limits of simplifying the real 3D problem to a 1D slab model to section 5). It is a fluid model, which seems reasonable given the large gas densities typical of MGI. The gas is assumed to be made of atoms of the same species as the plasma ions, with an atomic number $Z = 1$. Below, we simulate D_2 MGI into D^+ plasmas. We ignore, however, the existence of D_2 molecules and proceed as if the gas was made of D atoms, neglecting the dissociation energy of D_2 molecules (this seems reasonable since this energy is a factor 5 smaller than the ionization energy of two D atoms). The model consists of six equations describing the evolution of the electron density $n_{\rm e}$ (which, due to quasi-neutrality, is equal to the ion density $n_{\rm i}$) and temperature $T_{\rm e}$, the ion temperature $T_{\rm i}$ and the neutral density $n_{\rm n}$, velocity $V_{\rm n}$ and pressure $P_{\rm n}$, written here in conservative form:

$$\partial_t n_{\rm e} = n_{\rm e} n_{\rm n} I - n_{\rm e}^2 R + \partial_r (D \partial_r n_{\rm e}) \tag{1}$$

$$\partial_t (\frac{3}{2} n_{\rm e} e T_{\rm e}) = -n_{\rm e}(n_{\rm n} I E_{\rm ion} + n_{\rm n} L_{\rm lines} + n_{\rm e} R \frac{3}{2} e T_{\rm e}) - n_{\rm e}^2 L_{\rm brem+rec} + \partial_r (\chi n_{\rm e} \partial_r (e T_{\rm e})) \tag{2}$$

$$\partial_t (\frac{3}{2} n_{\rm e} e T_{\rm i}) = \frac{3}{2} n_{\rm e} (I P_{\rm n} - n_{\rm e} R e T_{\rm i} - \sigma_{\rm cx} V_{\rm cx} (n_{\rm n} e T_{\rm i} - P_{\rm n})) + \partial_r (\chi n_{\rm e} \partial_r (e T_{\rm i})) \tag{3}$$

$$\partial_t n_{\rm n} = -\partial_r (n_{\rm n} V_{\rm n}) - n_{\rm e} n_{\rm n} I + n_{\rm e}^2 R \tag{4}$$

$$\partial_t (m_{\rm n} n_{\rm n} V_{\rm n}) = -\partial_r (m_{\rm n} n_{\rm n} V_{\rm n}^2 + P_{\rm n}) - n_{\rm n} n_{\rm e} (I + \sigma_{\rm cx} V_{\rm cx}) m_{\rm n} V_{\rm n} \tag{5}$$

$$\partial_t (\frac{3}{2} P_{\rm n} + \frac{1}{2} m_{\rm n} n_{\rm n} V_{\rm n}^2) = -\partial_r (\frac{5}{2} P_{\rm n} V_{\rm n} + \frac{1}{2} m_{\rm n} n_{\rm n} V_{\rm n}^3) - n_{\rm n} n_{\rm e} (I + \sigma_{\rm cx} V_{\rm cx}) (\frac{3}{2} P_{\rm n}/n_{\rm n} + \frac{1}{2} m_{\rm n} V_{\rm n}^2) + n_{\rm e} (n_{\rm e} R + n_{\rm n} \sigma_{\rm cx} V_{\rm cx}) \frac{3}{2} e T_{\rm i} \tag{6}$$

In these equations, I, R and $\sigma_{\rm cx} V_{\rm cx}$ are the ionization, recombination and charge exchange rates, $E_{\rm ion}$ is the ionization energy and $L_{\rm lines}$ and $L_{\rm brem+rec}$ are the line and continuum (i.e. bremmstrahlung plus recombination) radiation rates. Details on these coefficients are given in section 2.3. All quantities are in SI units except temperatures which are in eV. D and χ are particle and heat diffusivities which are meant to represent turbulent transport. These two parameters are the only ad hoc parameters of the model and their effect is in fact limited. In the simulations below, we use $D = \chi = 1\,{\rm m}^2\,{\rm s}^{-1}$.

It is worth comparing our equations to those of the general non-linear fluid model for reacting plasma-neutral mixtures from Meier and Shumlak [26]. Equations (1)–(6) above correspond to equations (48)–(56) of [26] under the following assumptions/modifications: charged species are assumed to be at rest; scattering collisions are neglected; radiation losses are added; the term $\boldsymbol{R}_{in}^{\rm cx}$ is neglected; electron particle diffusion is added and electron and ion heat fluxes are treated as diffusive as a way to account for turbulent transport, as mentioned above.

The assumption of charged species being at rest is probably the most important one and deserves some discussion. As mentioned by Rozhansky *et al* [24], the gas tends to 'push' charged

species, i.e. to give rise to an $\boldsymbol{E}\times\boldsymbol{B}$ flow in the direction of the gas flow, but several mechanisms may damp this $\boldsymbol{E}\times\boldsymbol{B}$ flow. The physics involved is similar to the physics of pellet ablation clouds [25]. In the latter case, the strongest damping mechanism may be described as follows. The $\boldsymbol{E}\times\boldsymbol{B}$ flow is intimately related to an electric field $\boldsymbol{E}=-\nabla\Phi$ in the cloud. If a field line connects the top and the bottom of the cloud (after a certain number of toroidal turns), the potential difference $\Delta\Phi$ between its extremities will drive a parallel current. The current path will be closed (it has to be for quasi-neutrality to pertain) by a polarization current proportional to $\mathrm{d}\boldsymbol{E}/\mathrm{d}t$ circulating inside the cloud. The latter is associated to a reduction of $|\boldsymbol{E}|$ and therefore a damping of the flow. This mechanism, which is already strong for pellet ablation clouds, is likely to be even stronger in the MGI case because of the larger cloud poloidal extent. Note that this mechanism, introduced by Pégourié *et al* in [25], was not included in the slightly older work of Rozhansky *et al* [24]. For simplicity we assume here that this braking mechanism is strong enough that charged species remain at rest. The question may however be addressed in future work by including a momentum equation for charged species in our model. Looking at the above equations, one may notice that the term $-n_\mathrm{e}(I+\langle\sigma v\rangle_\mathrm{cx})\frac{1}{2}m_\mathrm{n}n_\mathrm{n}V_\mathrm{n}^2$ in the neutral energy equation (equation (6)), which represents kinetic energy transferred from neutrals to ions due to ionization and charge exchange, has no counterpart in the ion energy equation (equation (3)). This is because this term is associated to a momentum transfer between neutrals and ions, and this momentum is assumed to be annihilated by the braking force(s) acting on charged species. Consistently, the associated energy is assumed to be annihilated by the work of the braking force(s). Of course, in reality, the energy has to go somewhere, possibly into heat in the coils or passive structures, or in the plasma itself. In any case, since this energy is small compared to the thermal energy of the plasma, it is probably justified to assume that it is simply annihilated.

2.2. Initial and boundary conditions

One key feature of our model is to treat in a unified way the plasma, the vacuum region and the gas reservoir: the above equations apply throughout these three domains and the simulations cover the gas propagation into the vacuum and its interaction with the plasma, as will be presented in section 3.

Boundary conditions are null gradients for all fields at the center of the plasma ($r=0$) and $V_\mathrm{n}=0$ at the end of the gas reservoir ($r=r_\mathrm{max}$).

Initial conditions for n_e, T_e and T_i are typically set according to pre-MGI experimental measurements. Initial conditions for n_n and P_n are a finite and homogeneous value in the reservoir and 0 elsewhere, while $V_\mathrm{n}=0$ everywhere. The initial values of n_n and P_n in the reservoir, as well as the radial extent of the reservoir in the simulation, are chosen so as to match three critical experimental quantities: the initial number of D atoms and the sound velocity $c_\mathrm{s,res}$ inside the reservoir and the initial flux of atoms out of it (technical details are given in the appendix). This allows reproducing the gas flow in the vacuum region, as we shall see below.

Since the model contains no heat or particle source in the plasma, plasma profiles evolve in time, even before the gas arrives. For hot plasmas, this is not a problem since the evolution is much slower than the timescale of the physics under study. However, for cold plasmas like those simulated in section 4, this is a problem. Typically, a radiative collapse may happen before the gas reaches the plasma. The solution adopted in section 4 has been to turn off recombination and radiation terms.

2.3. Atomic physics coefficients

Coefficients I, R, L_lines and $L_\mathrm{brem+rec}$ are taken from the ADAS database [27], where they are given as function of n_e and T_e. They are represented in figure 1.

For the charge exchange rate $\sigma_\mathrm{cx}V_\mathrm{cx}$, we use the expressions given in Meier and Shumlack [26] (which apply to hydrogen but we assume that deuterium is similar): $\sigma_\mathrm{cx}[m^2]=1.09\times10^{-18}-7.15\times10^{-20}\ln(V_\mathrm{cx})$ (see section III.D.2 in [26]) and $V_\mathrm{cx}=(\frac{4}{\pi}v_\mathrm{Ti}^2+\frac{4}{\pi}v_\mathrm{Tn}^2+V_\mathrm{n}^2)^{1/2}$ (equation (17) in [26]), where $v_{T\alpha}\simeq(2eT_\alpha/m_\alpha)^{1/2}$ is the thermal velocity of species α. Figure 2 shows $\sigma_\mathrm{cx}V_\mathrm{cx}$ as a function of T_i, assuming that v_Tn and V_n are negligible.

2.4. The IMAGINE code

Equations (1) to (6) have been implemented in a new code called IMAGINE. A MUSCL scheme (monotonic upstream-centered scheme for conservation laws) is used to advance the neutral equations ignoring the atomic physics terms. The MUSCL scheme is a finite volume method providing highly accurate numerical solutions even when the solutions exhibit shocks or discontinuities (which is the case here). The part related to atomic physics is advanced separately with an explicit scheme. The equations for electrons and ions are advanced with an explicit conservative scheme.

3. Simulation of a D_2 MGI into a JET Ohmic plasma

In this section, we present IMAGINE simulations of MGI into a 'hot' plasma. Section 4 will deal with simulations of MGI into a 'cold' plasma.

3.1. Description of the experiment

We simulate JET pulse 86887. This is an Ohmic D plasma pulse with $B_t=2$ T, $I_p=2$ MA, $q_{95}=2.9$ in which a disruption was triggered on a 'healthy' plasma by activating the disruption mitigation valve number 2 (DMV2). Note that the same pulse has been modelled with the 3D non-linear MHD code JOREK, as reported in [23, 35].

Electron density and temperature profiles just before the DMV2 trigger are shown in figure 3 together with fits of these profiles used as initial conditions in IMAGINE simulations.

In this pulse, DMV2 was pre-loaded with D_2 at 5 bar, which represents $1.2\cdot10^{23}$ D_2 molecules (the volume of the DMV2 reservoir being $V_\mathrm{res}=1$ l and its temperature $\simeq300$ K), i.e.

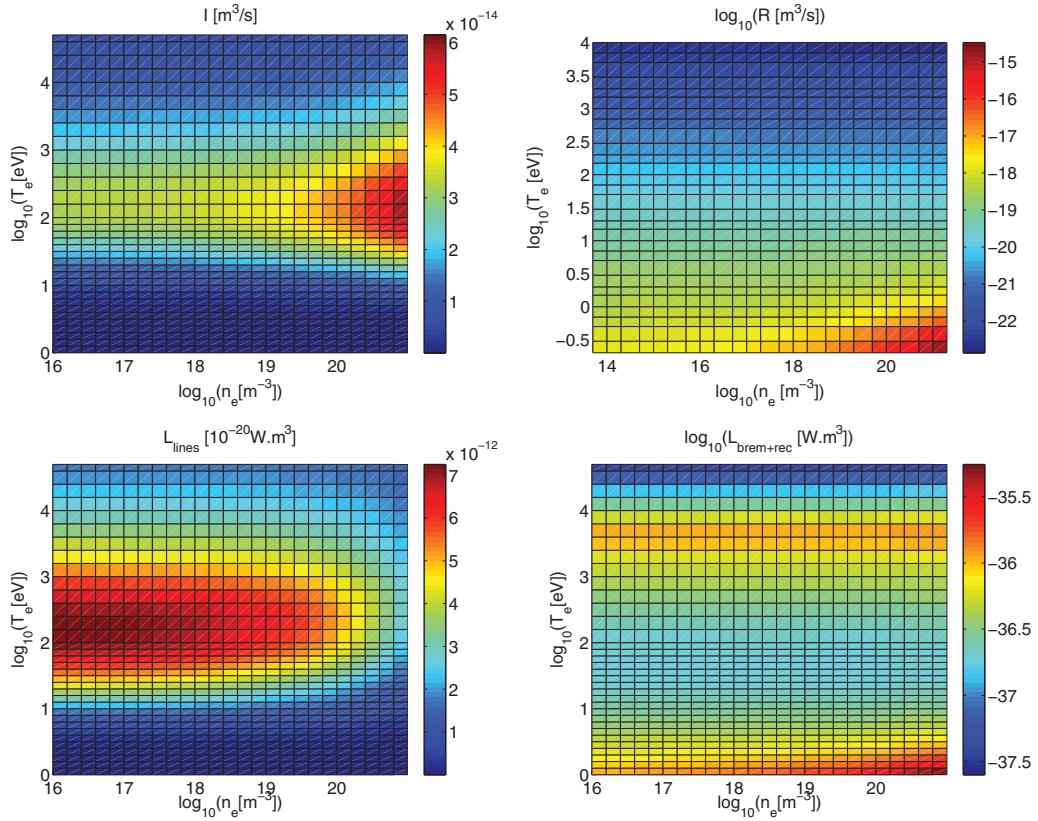

Figure 1. Atomic physics coefficients for deuterium from the ADAS database.

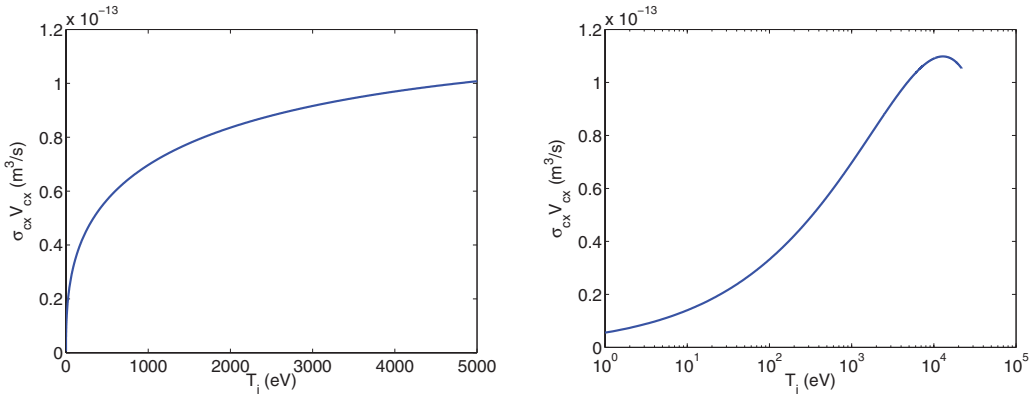

Figure 2. $D - D^+$ charge exchange rate $\sigma_{cx}V_{cx}$ as a function of T_i (left: linear scale; right: logarithmic scale), assuming that v_{Tn} and V_n are negligible (see text for explanation).

roughly 100 times the initial D nuclei content of the plasma. After the valve opening, the gas propagates towards the plasma via a guiding tube of length $L_{tube} = 2.36$ m. The gas is then delivered at the midplane of Octant 3, as shown in figure 4. This figure also gives information on the position of diagnostics relevant to this paper, in particular vertical interferometry lines, which are located in Octant 7, i.e. opposite to DMV2. Figure 5 shows an overview of the disruption phase. First effects of the MGI are visible from about 2 ms (relative to the DMV2 trigger) in the form of increases in the line integrated density and radiated power. The thermal quench occurs at about 12 ms as can be seen from the fast collapse of the soft x-ray (SXR) signal accompanied by a burst of MHD activity and immediately followed by the characteristic I_p spike. The current quench ensues.

3.2. Simulation results

We shall now describe the IMAGINE simulation results, starting with the propagation of the gas into the vacuum region (i.e. the guiding tube).

3.2.1. Gas propagation into the vacuum region. In laboratory experiments, Bozhenkov *et al* have found that the gas flow in the guiding tube is well described by the analytical solution of the 1D Euler equations with an infinite reservoir, under the condition that $\frac{d}{c_{s,res} \cdot t} > 0.6$, where d is the distance to the reservoir [9]. This type of flow is called a 'rarefaction wave'. Since in the vacuum region the equations of IMAGINE boil down to the 1D Euler equations, we recover this flow in the simulations.

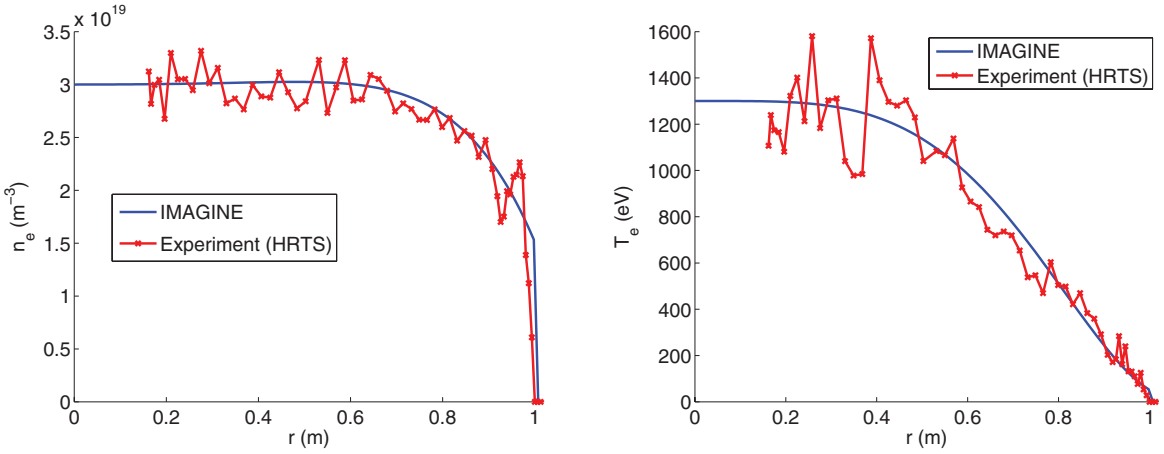

Figure 3. Experimental n_e (left) and T_e (right) profiles for JET pulse 86887 from high resolution Thomson scattering (HRTS) just before the DMV2 trigger (red crosses) and fits of these profiles used as initial conditions in IMAGINE (blue). (Note: the HRTS data has been remapped onto an EFIT equilibrium. The radial coordinate r used in the above profiles is defined as $a \cdot \psi_n^{0.5}$, with $a = 1$ m, where ψ_n is the normalized poloidal flux from EFIT.).

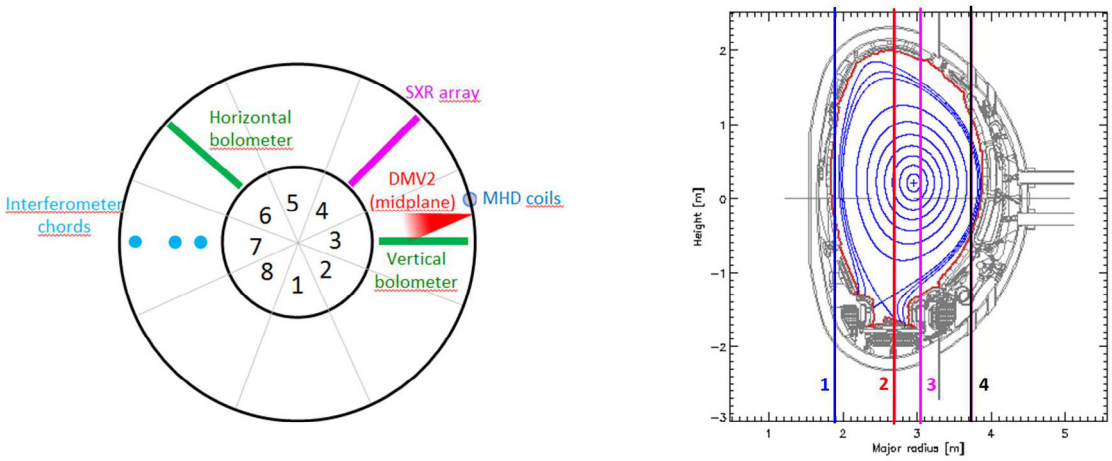

Figure 4. Left: schematic view of JET from the top, indicating octant numbers and the location of DMV2 and diagnostics used in figure 5. Right: poloidal cross-section showing magnetic flux contours from EFIT reconstruction just before the triggering of DMV2 and the interferometry vertical lines of sight.

Figure 6 (left) shows successive neutral density profiles calculated by IMAGINE. One can observe the typical self-similar behaviour of the rarefaction wave [9]. Figure 6 (right) shows the flux of D_2 molecules across $r = 3$ m, comparing IMAGINE and the analytical solution (given explicitly in [9]). A good match (with a difference $< 10\%$) can be observed up to about 3 ms, from which point the IMAGINE solution starts to decrease due to the depletion of the reservoir—in contrast with the analytical solution, which assumes an infinite reservoir.

In figure 6 (left), the reader may notice that the reservoir in IMAGINE has a radial extent of about 1.5 m, which is much larger than the typical dimension of the actual reservoir, whose volume is $V_{res} = 11$. Reasons for this are detailed in the appendix. One consequence is that the pressure equilibration time in the reservoir is much longer in the simulations than in the experiment. This must lead to a slightly inexact description of the gas flow. The real gas flux probably has a smoother behaviour, with no abrupt change at 3 ms as in figure 6 (right). However, the discrepancy is probably not very large and, as stated above, the early gas flow calculated by IMAGINE matches well the laboratory measurements of Bozhenkov *et al*, giving confidence in the following results (which essentially have to do with the *early* interaction of the gas with the plasma).

Let us now focus on what happens when the gas reaches the plasma. Here, charge exchange and recombination play a central role. In order to demonstrate this, we will first present a simulation without these effects and then a simulation with these effects.

3.2.2. Gas penetration into the plasma, neglecting charge exchange and recombination. Without charge exchange and recombination, the gas penetrates easily into the plasma. This is apparent in figure 7 (top left), which shows profiles of the neutral velocity V_n at different times: the gas flow is not affected as the gas enters the plasma. On the neutral density profiles shown in figure 7 (top right), one can see that the tip of the rarefaction wave is 'eaten' by ionisation. This causes a dramatic increase in n_e, which reaches values on the order of $2 \cdot 10^{21}$ m^{-3}, as can be seen in figure 7 (bottom left) (note the logarithmic scale in this figure). This increase

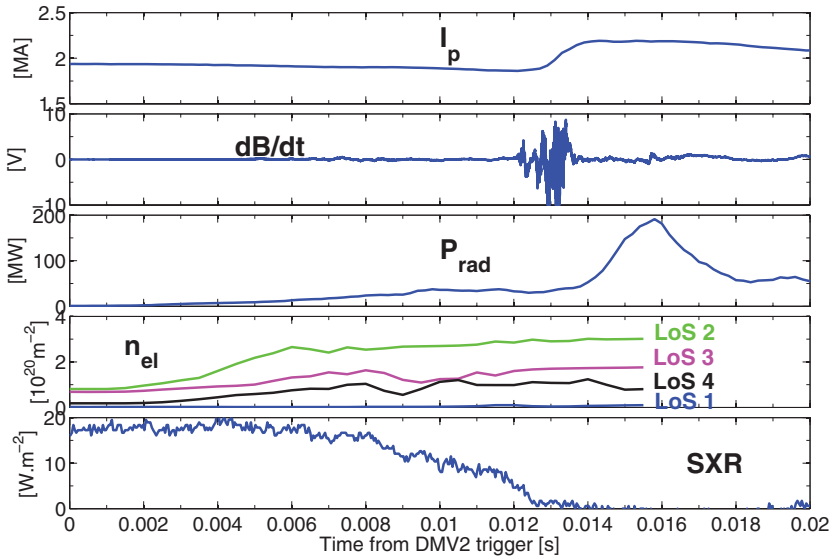

Figure 5. Experimental time traces for JET pulse 86887, from top to bottom: plasma current I_p, magnetic fluctuations from Mirnov coil, radiated power from bolometry, line integrated density from interferometry, and soft x-rays signal from a central chord (see figure 4 for information on the diagnostics position). The time origin corresponds to the DMV2 trigger.

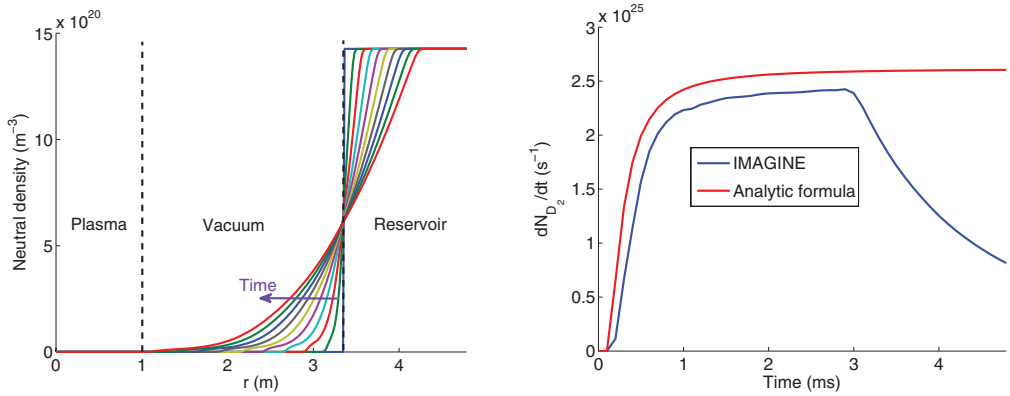

Figure 6. Left: successive neutral density profiles (separated by 0.1 ms) from IMAGINE simulation. Right: flux of D_2 molecules in vacuum across $r = 3$ m as found with IMAGINE and with the analytical solution of the 1D Euler equations.

in n_e is clearly incompatible with experimental data, as can be seen in figure 8, which compares experimental and synthetic interferometry data. In this figure, the synthetic data is calculated from the output of IMAGINE as $n_{el} = 2\int_0^a n_e dr$ (the factor 2 comes from the fact that the experimental measurement corresponds to $\int_{-a}^{a} n_e dr = 2\int_0^a n_e dr$), and compared with experimental measurements from lines of sight 2 and 3 of the interferometer, which are rather central, as can be seen in figure 8 (right). Note that the comparison is meaningful only if the experimental n_e is relatively homogeneous on flux surfaces. This may indeed be the case, due to the fast parallel expansion of the over-density created by the MGI. For example, JOREK simulations [23] find a parallel expansion velocity $v_\parallel \simeq 30$ km $\cdot$ s^{-1}, corresponding to a density homogenization time $\tau \simeq \frac{2\pi qR}{v_\parallel} \simeq 2$ ms. In figure 8, the synthetic signal from the IMAGINE simulation without charge exchange and recombination goes beyond the axis limit at about 2.5 ms and continues increasing dramatically later, reaching values one order of magnitude higher than the experimental ones, clearly indicating that some assumptions of the model must be wrong. This process is accompanied by the penetration of a very sharp cold front, as can be seen in figure 7 (bottom right). The cooling is mostly due to dilution, since n_e increases by roughly 2 orders of magnitude. It can be seen that within 1.5 ms from the DMV2 trigger, the cold front has reached $r = 0.9$ m, which corresponds to the $q = 2$ surface, and within 4 ms it has reached mid-radius. This is also incompatible with experimental data since the TQ is observed about 12 ms after the DMV2 trigger. Recall that in several machines, the TQ has been observed to occur when the cold front reaches the $q = 2$ surface [6–8], and even though there is not clear experimental evidence for this fact in JET, JOREK modelling suggests that this is the case too [23, 35].

To summarize, when neglecting charge exchange and recombination, the gas and the cold front penetrate much too fast and easily compared to the experiment.

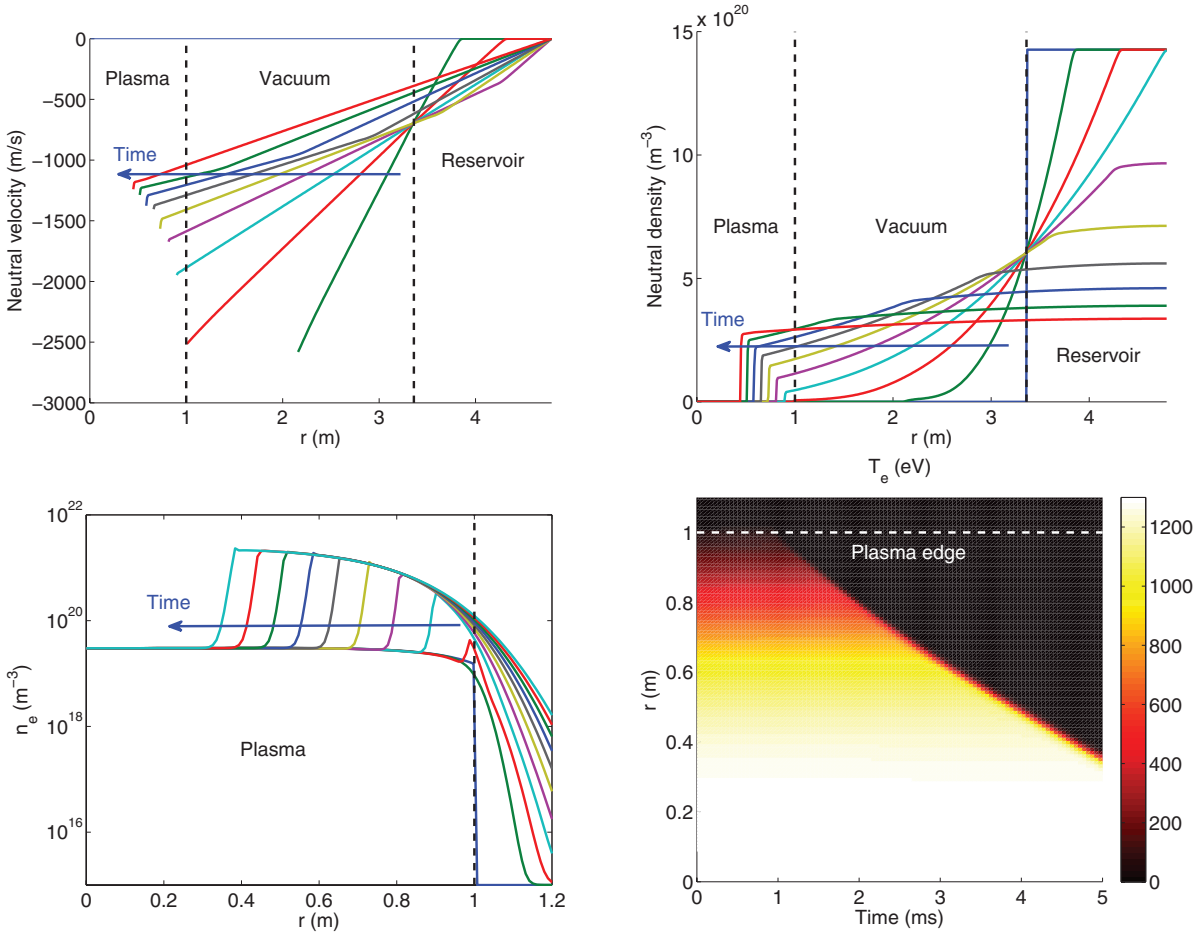

Figure 7. Successive profiles of neutral velocity V_n (top left), neutral density n_n (top right), and electron density n_e (bottom left), separated by 0.5 ms; electron temperature T_e versus time and radius (bottom right).

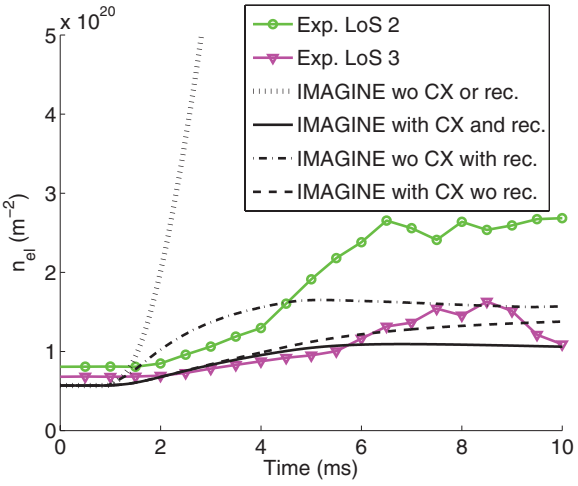

Figure 8. Comparison between experimental and synthetic interferometry data (see figure 4 to visualize the interferometry lines of sight).

3.2.3. Gas penetration into the plasma, including charge exchange and recombination. Turning on the charge exchange and recombination terms changes the situation drastically: the gas flow is now rapidly stopped at the edge of the plasma and a shock wave is created which propagates away from the plasma, as is clearly visible on the successive neutral velocity (V_n) and density (n_n) profiles from figure 9 (top left and right plots). Concerning the shock wave, it is good to check whether Rankine–Hugoniot jump conditions [28] are satisfied in the simulation. Figure 10 shows that this is the case: while n_n is discontinuous across the shock (top left plot), the quantities $\rho_n(V_n - V_{shock})$ (top right), $\rho_n V_n(V_n - V_{shock}) + P_n$ (bottom left) and $(V_n - V_{shock})(\frac{P_n}{\gamma - 1} + \frac{1}{2}\rho_n V_n^2) + V_n P_n$ (bottom right) are continuous (where $\rho_n = m_n n_n$), in agreement with the conservation of mass, momentum and energy density. This indicates that IMAGINE resolves the shock wave appropriately.

As a result of the strong braking, only a small fraction of the gas penetrates into the plasma and the n_e increase is therefore much more modest than in the previous simulation. Still, n_e increases by a factor $\simeq 6$ at $r = 0.9$ m, as can be seen in figure 9 (bottom left plot). Looking at figure 8 again, this simulation (plain line) appears much more consistent with interferometry data than the previous one: the n_{el} increase now has the right order of magnitude. Figure 9 (bottom right) indicates that the cold front is less sharp and penetrates much more slowly than in the previous simulation. It takes about 5–10 ms for it to reach the $q = 2$ surface ($r = 0.9$ m), which is compatible with the experimental TQ onset time of 11 ms. In conclusion, when including charge exchange and recombination,

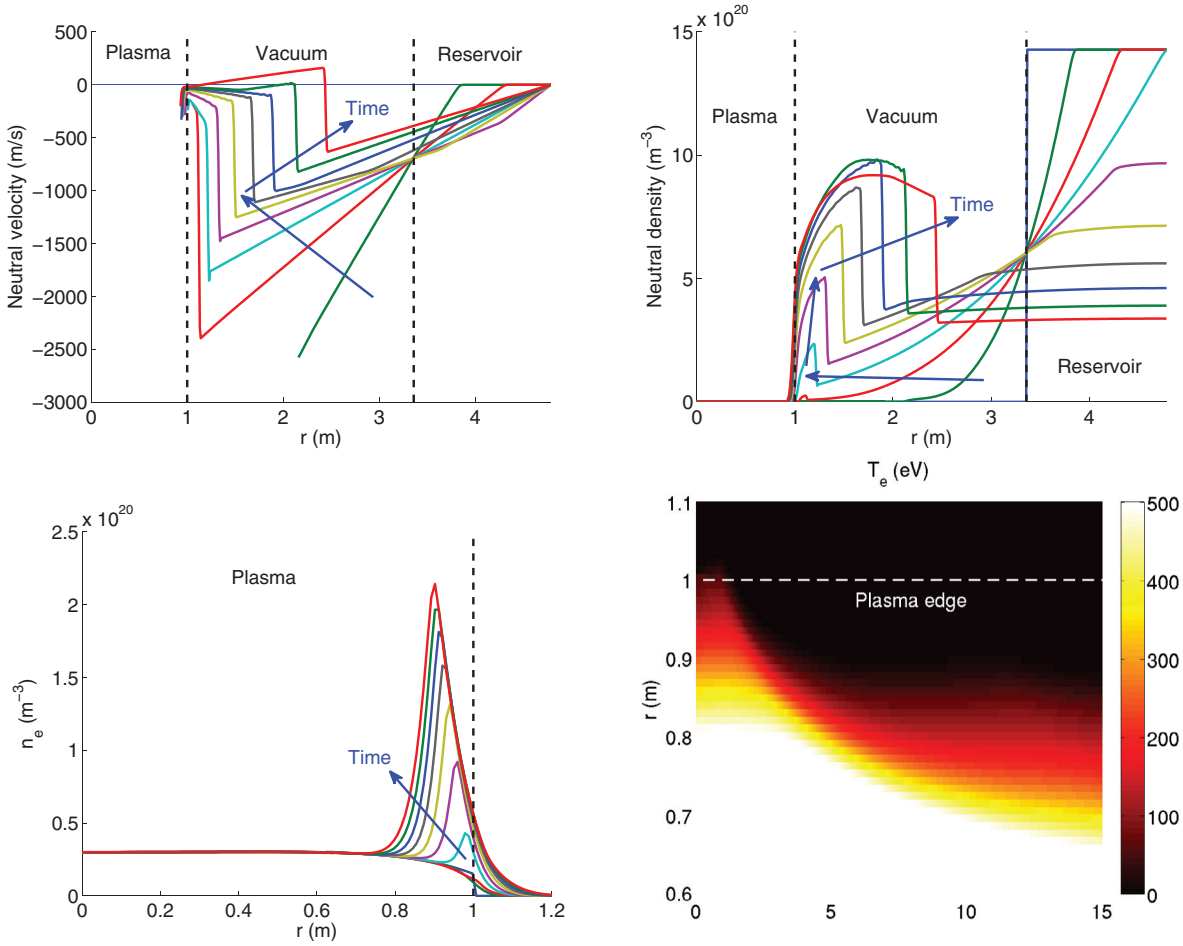

Figure 9. Successive profiles of neutral velocity V_n (top left), neutral density n_n (top right), and electron density n_e (bottom left), separated by 0.5 ms; electron temperature T_e versus time and radius (bottom right).

IMAGINE simulations are rather consistent with experimental measurements. Let us now interpret these results.

3.3. Interpretation and discussion

The above simulations demonstrate the crucial role of charge exchange and recombination in promptly braking the gas, limiting its penetration into the plasma and giving rise to a shock wave propagating away from the plasma. In order to identify the mechanisms responsible for this braking, let us consider the equation for the evolution of V_n (which can be derived from equations (4) and (5)):

$$m_\mathrm{n} n_\mathrm{n} \mathrm{d}_t V_\mathrm{n} = -\partial_r P_\mathrm{n} - (n_\mathrm{e}^2 R + n_\mathrm{e} n_\mathrm{n} \sigma_\mathrm{cx} V_\mathrm{cx}) m_\mathrm{n} V_\mathrm{n}. \qquad (7)$$

Here, $\mathrm{d}_t = \partial_t + V_\mathrm{n}\partial_r$. This equation shows that the neutral velocity is influenced by the neutral pressure gradient and by a friction force $(n_\mathrm{e}^2 R + n_\mathrm{e} n_\mathrm{n} \sigma_\mathrm{cx} V_\mathrm{cx}) m_\mathrm{n} V_\mathrm{n}$. The latter comes from the fact that each charge exchange or recombination creates a neutral which, on average, is at rest, thereby decreasing the average neutral velocity V_n by a quantity proportional to $V_\mathrm{n}/n_\mathrm{n}$. Regarding the former, let us consider the equation for the evolution of P_n (which can be derived from equations (4)–(6)):

$$\partial_t P_\mathrm{n} = -V_\mathrm{n}\partial_r P_\mathrm{n} - \frac{5}{3} P_\mathrm{n} \partial_r V_\mathrm{n} + n_\mathrm{n} n_\mathrm{e} \sigma_\mathrm{cx} V_\mathrm{cx} \left(\frac{1}{3} m_\mathrm{n} V_\mathrm{n}^2 + e T_\mathrm{i} - \frac{P_\mathrm{n}}{n_\mathrm{n}} \right) + n_\mathrm{e}^2 R \left(\frac{1}{3} m_\mathrm{n} V_\mathrm{n}^2 + e T_\mathrm{i} \right) - n_\mathrm{e} I P_\mathrm{n} \qquad (8)$$

It appears that charge exchange and recombination tend to increase P_n via (among others) terms proportional to eT_i. This is due to the fact that each charge exchange or recombination creates a neutral whose energy, on average, is equal to $\frac{3}{2} eT_\mathrm{i}$. This effect typically leads to the formation of a P_n spike at the gas–plasma interface. The $-\partial_r P_\mathrm{n}$ term in equation (7) then tends to accelerate the gas on the inside of this spike and decelerate it on the outside. From a kinetic point of view, this may be understood as hot neutrals being created with a velocity pointing randomly either toward the plasma core or away from it (depending on the gyro-angle of the ion just before the charge exchange or recombination).

In summary, charge exchange and recombination influence the gas flow in two ways: via a friction force and via gas heating. The relative importance of these two mechanisms depends on the ion temperature. We will come back to this point in section 4.

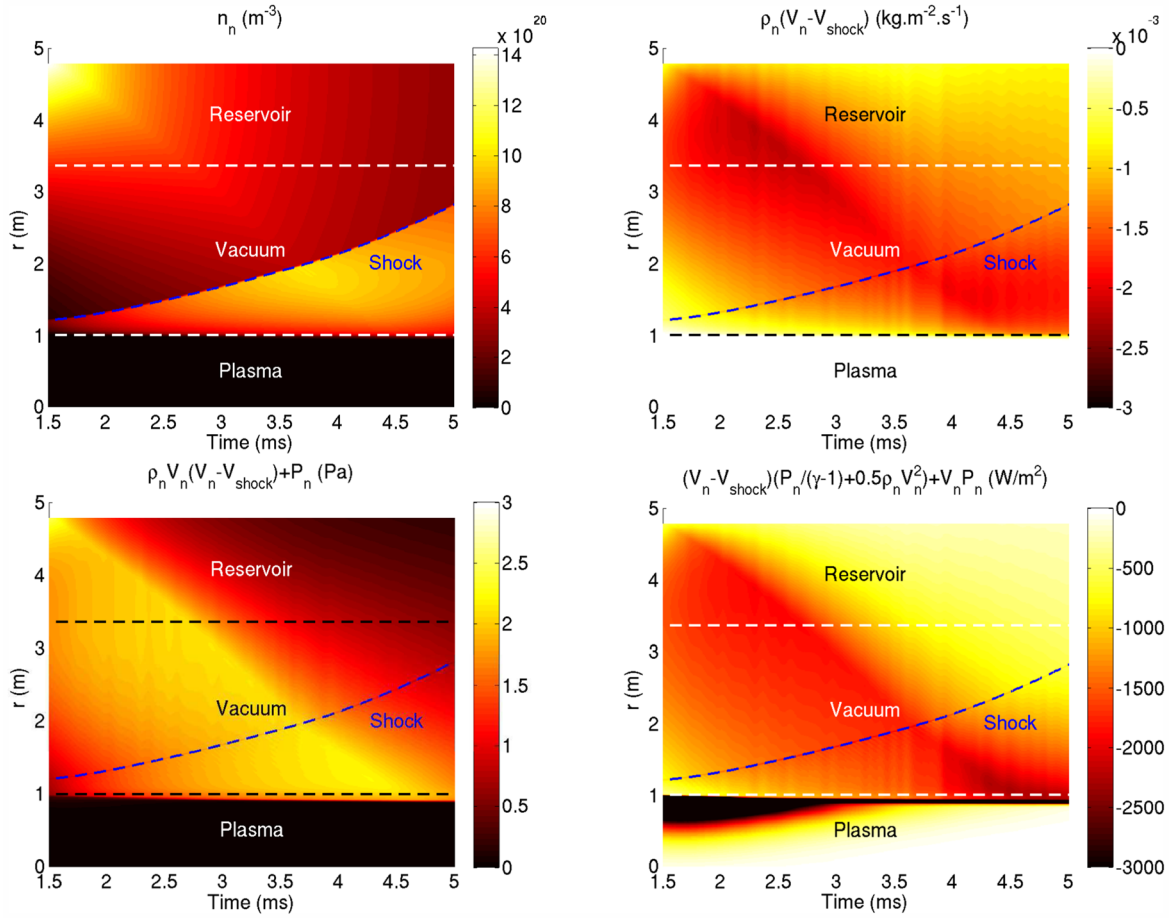

Figure 10. Verification of the Rankine–Hugoniot (RH) jump conditions: the shock (blue dashed line) corresponds to a discontinuity on the neutral density (top left) but not on $\rho_n(V_n - V_{shock})$ (top right), $\rho_n V_n(V_n - V_{shock}) + P_n$ (bottom left) or $(V_n - V_{shock})(\frac{P_n}{\gamma - 1} + \frac{1}{2}\rho_n V_n^2) + V_n P_n$ (bottom right), in agreement with the RH conditions.

The fact that a shock wave should appear when the gas reaches the plasma has been predicted already by Parks and Wu [29], who state (at the beginning of section 3 of [29]) that 'The plasma pressure impresses on the frontal surface driving a shock wave running inwards and backwards'. In our opinion, this statement may be misleading since the plasma pressure does not directly apply on the gas. However, the gas heating effect described above may be seen as a conversion of plasma pressure into neutral pressure and in that sense, plasma pressure may be considered to indirectly impress on the gas. But the above discussion shows that this is not the only type of interaction between the plasma and the gas: the frictional interaction should not be forgotten.

Another question is whether there is a dominant player between charge exchange and recombination. A partial answer is provided in figure 8 (left), which contains simulation results with charge exchange and recombination turned off separately. This figure indicates that charge exchange has a stronger effect than recombination, but the most important point is probably that each of these two effects is strong enough to significantly brake the gas and create a shock wave by itself.

Finally, it is important to note that the radiated power in the above IMAGINE simulation is of order 0.5 MW, which is more than one order of magnitude smaller than what is measured experimentally (see figure 5). The measured radiated power probably comes from background impurities present in the target plasma. Spectroscopy data actually shows that Argon is present in this pulse [30], which is probably a consequence of the Argon MGI performed in a previous pulse in the session. Thus, what may happen in reality is that T_e is lowered first by dilution due to the D_2 MGI, and then, once T_e is low enough, Argon radiates away the energy. It could be that this effect eases the penetration of the gas, but it is not obvious to what extent it may do so. The fact that the simulation already agrees with experimental observations in terms of gas penetration speed suggests that this effect is not very strong. This point could be addressed in future work by adding background impurities in IMAGINE.

4. Gas penetration into the background plasma surrounding a runaway beam

As mentioned in the introduction, multiple attempts to 'kill' an RE beam with MGI (including with high Z gases like Kr or Xe) in JET have shown no effect [1]. A possible explanation

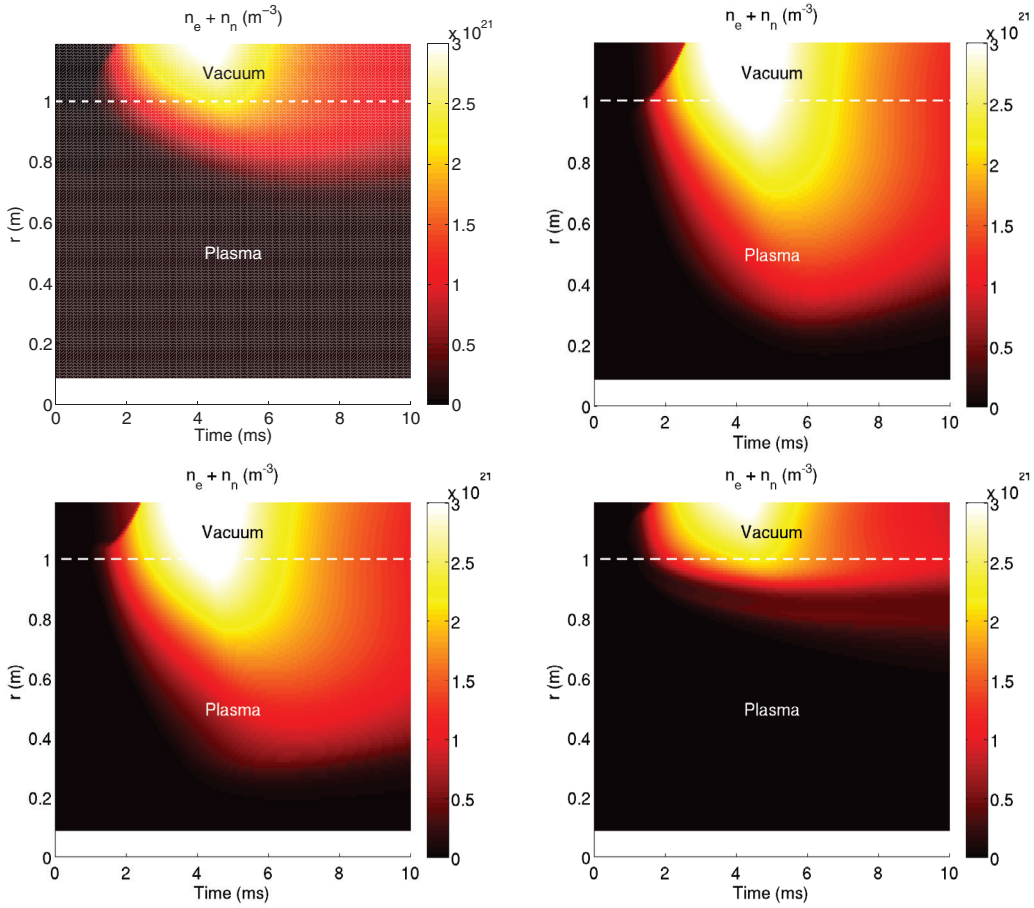

Figure 11. Electron plus neutral density as a function of time and radius for $n^0_{e,bg} = 10^{20}$ m^{-3}, $T^0_{e,bg} = 2$ eV (top left); $n^0_{e,bg} = 10^{19}$ m^{-3}, $T^0_{e,bg} = 2$ eV (top right); $n^0_{e,bg} = 10^{19}$ m^{-3}, $T^0_{e,bg} = 20$ eV (bottom left); $n^0_{e,bg} = 10^{19}$ m^{-3}, $T^0_{e,bg} = 2$ keV (bottom right).

may be that the RE beam, which is localized in the core of the plasma, extending perhaps up to mid-radius, is 'shielded' by the cold background plasma surrounding it via a gas braking effect similar to the one described above. However, it is essential to note that on Tore Supra [31], DIII-D [32] or ASDEX-U [33], MGI clearly affects the RE beam, so the gas must reach the beam in these machines. It is therefore interesting to investigate possible reasons for differences in terms of gas penetration between the machines.

The electron density $n_{e,bg}$ and temperature $T_{e,bg}$ of the background plasma are one possibility. Although measurements are not easy (especially for temperature), $n_{e,bg}$ seems to be typically a few 10^{20} m^{-3} in JET and DIII-D and a few 10^{19} m^{-3} in Tore Supra and ASDEX-U, and $T_{e,bg}$ is estimated to be at least 20 eV in JET while $T_{e,bg} \sim 2$ eV in DIII-D and ASDEX-U [1, 32, 33]. The background plasma therefore seems to be denser and/or hotter in JET than in DIII-D or ASDEX-U. IMAGINE allows investigating how gas penetration depends on $n_{e,bg}$ and $T_{e,bg}$. For this purpose, we made simulations of D_2 MGI in JET from DMV2 at 20 bar. This setting was chosen because it corresponds to an actual pulse. The n_e and T_e profiles were scaled from the profiles of the Ohmic pulse 86887 modelled above. We assumed $T_i = T_e$ for the initial profiles. We also turned off the radiation and recombination terms. Indeed, due to the low T_e and to the absence of certain physical effects in the model (e.g. Joule heating), the bulk plasma may otherwise undergo a radiative collapse and/or significant recombination over the timescale of the simulation, which are not the purpose of the present study. Figure 11 presents the evolution of the sum of free plus bound electrons, i.e. $n_e + n_n$, versus time and radius, for four simulations: (A) $n^0_{e,bg} = 10^{20}$ m^{-3}, $T^0_{e,bg} = 2$ eV (top left); (B) $n^0_{e,bg} = 10^{19}$ m^{-3}, $T^0_{e,bg} = 2$ eV (top right); (C) $n^0_{e,bg} = 10^{19}$ m^{-3}, $T^0_{e,bg} = 20$ eV (bottom left); (D) $n^0_{e,bg} = 10^{19}$ m^{-3}, $T^0_{e,bg} = 2$ keV (bottom right). The superscript 0 denotes the central value at the beginning of the simulation. We chose to represent $n_e + n_n$ because both free and bound electrons may brake RE (although not exactly to the same extent). Simulation (A) shows that even at very low $T_{e,bg}$, the gas is prevented from penetrating far into the plasma if $n_{e,bg}$ is large enough. The mechanism responsible for this is gas–plasma friction due to charge exchange, which remains significant even at very low plasma temperatures due to the weak T_i dependency of $\sigma_{cx}V_{cx}$ at low T_i, visible in figure 2 (right). At lower densities, however, such as in simulation (B), the gas may penetrate much further. This is easily understood as the friction force is proportional to n_e. Simulations (B), (C) and (D) constitute a scan in $T^0_{e,bg}$ at fixed $n^0_{e,bg} = 10^{19}$ m^{-3}. Moving from $T^0_{e,bg} = 2$ eV to $T^0_{e,bg} = 20$ eV, i.e. from (B) and (C), has almost no influence on the result, whereas at $T^0_{e,bg} = 2$ keV (case (D)), gas penetration is clearly hindered. This is

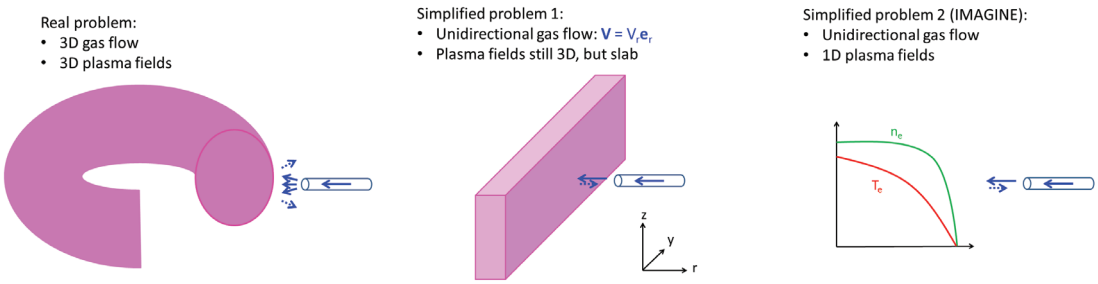

Figure 12. The simplification from the real 3D problem (left) to the IMAGINE model (right) may be viewed as a two step process (with the intermediate step shown in the middle).

due to the T_i dependency of the abovementioned mechanism of gas braking via charge exchange heating: for $T^0_{e,bg} < 20$ eV, this mechanism plays an almost negligible role, whereas for $T^0_{e,bg} = 2$ keV, it is the dominant player. The simulations therefore reveal an important difference in gas penetration physics between a hot and a cold target plasma: in the former case, the gas is mainly braked via heating while in the latter, it is mainly braked by friction. We note that friction had been neglected in the work of Parks and Wu [29] which may have led to a significant overestimation of the gas penetration depth into an ITER CQ plasma.

It may be that the situation at JET corresponds to simulation (A), where the superficial penetration of the gas would be insufficient to affect the RE beam if the latter is localized inside, say, $r/a \simeq 0.5$. The lower $n^0_{e,bg}$ at Tore Supra and ASDEX-U may on the other hand correspond to simulation (C), where one would expect the gas to affect the beam. Simulation results, however, do not provide an obvious explanation for the difference between JET and DIII-D, since $n^0_{e,bg}$ has the same order of magnitude in these two machines and the factor ~ 10 difference in terms of $T^0_{e,bg}$ is not expected to affect gas penetration significantly. Of course, it may be that the explanation lies somewhere else, for example in a machine size effect (a larger machine means a thicker background plasma 'shield' around the RE beam) or different MGI settings. Investigating these possibilities is left for future work. For now, the important practical conclusion of our study in view of further experiments in JET is that optimizing the RE beam production 'recipe' in order to lower $n^0_{e,bg}$ may help get an effect of MGI on the beam.

To finish this section, we would like to draw attention to an interesting observation made in the abovementioned Tore Supra experiment. Figure 7(b) in [31] shows that the neutral pressure measured with a pressure gauge in the vacuum vessel decreases abruptly from $\simeq 2.5$ Pa to $\simeq 1$ Pa in about 20 ms (which is the response time of the gauge) just after the extinction of the plasma, after which it stabilizes slightly below 1 Pa, the latter being the expected pressure for a uniform filling of the vessel at the vessel temperature of 120 °C. The pressure of $\simeq 2.5$ Pa in the runaway plateau phase suggests that the gas is confined to a smaller volume and/or hotter than 120 °C. This is consistent with the findings presented in this paper that gas–plasma interaction prevents most of the gas from penetrating the plasma volume (even when part of the gas does penetrate the plasma and affects the runaway beam) and also heats up the gas. An interesting direction for future work is to investigate the possible role of this gas surrounding the plasma. This question cannot be addressed by a simple 1D model like the one used in IMAGINE.

5. Discussion on the justifiability and limits of the 1D model

Now that we have seen the physics displayed by IMAGINE, it is time to discuss the justifiability and limits of the 1D model.

It is useful to think of the simplification from the real 3D problem to the 1D model as a two step process, as illustrated in figure 12. Step 1 consists in going from a toroidal to a slab geometry (but still with 3D fields) and assuming that the gas flow is directed purely along the radial direction. This gives the same set of equations as equations (1) to (6) but with all variables being local (i.e. functions of (r,y,z) using the coordinate system shown in figure 12). Step 2 then consists in assuming that plasma quantities are homogeneous on flux surfaces and that the neutral density and pressure are localized in the y and z directions. By performing flux surface averages of the equations obtained at Step 1, one gets equations (1) to (6). Note that in these equations, n_n (P_n) represents the flux surface average of the neutral density (pressure), but there is no need to assume that the neutral density or pressure is homogeneous on flux surfaces. It suffices to assume that the gas cloud is localized in space (i.e. that n_n and P_n are gate-like functions of (y,z)). On the other hand, V_n represents the velocity of the gas *in the region where there is gas* and not a flux surface average.

Let us now discuss the justifiability and consequences of each of the two steps. Concerning Step 1, the justifiability of the assumption that the gas flow is directed purely along the radial direction is connected to the smallness of the ratio $L_{plasma\text{-}tube}/D_{tube}$, where $L_{plasma\text{-}tube}$ is the distance between the exit of the gas guiding tube and the plasma, and D_{tube} is the tube diameter. In the case of JET DMV2, this ratio is about 3 ($L_{plasma\text{-}tube} \simeq 0.5$ m and $D_{tube} \simeq 0.15$ m), which is not a small value. This means that the gas can expand significantly between the exit of the tube and the plasma, but this may not be an important problem since the procedure described above to derive the IMAGINE equations does not forbid the cross-section (in the (y,z) plane) of the gas cloud to

change with r. On the other hand, this also means that while in IMAGINE, the shock wave produced by the plasma–gas interaction has no choice but to go back into the guiding tube, in reality it may not (or not fully) do so since it may go to the side. This must lead to an overestimation of the effect of the shock wave and therefore an underestimation of the gas penetration depth in IMAGINE. The justifiability of the other simplification made in Step 1, i.e. the use of a slab geometry, is connected to the penetration depth of the gas: in cases where the gas penetrates deep into the plasma, IMAGINE must underestimate the penetration since the use of a slab geometry means that in IMAGINE, the gas interacts with increasingly more plasma than there really is as it progresses toward the center of the plasma. For shallow gas penetration, the slab approximation is better justified.

Step 2 assumes that plasma quantities are homogeneous on flux surfaces. In the region where there is no gas, this may be valid since the homogenization time $\pi qR/c_{s,ion}$ is of order $10^{-4} - 10^{-3}$ s for JET (for ion temperatures between 1 and 100 eV), which is shorter than or comparable to the gas penetration time. But assuming homogeneous plasma quantities on flux surfaces also implies that the plasma and the gas interpenetrate. Whether this is true or not is an important question. A typical flux-surface-averaged neutral density in the simulations shown in figure 11 is 10^{21} m^{-3}. Assuming a cross-section of the gas flow of 0.2 m^2, which must be representative of the moment when the gas reaches the edge of the plasma, this translates to a 'real' neutral density of order $5 \cdot 10^{23}$ m^{-3}. A typical value for the charge-exchange cross-section (see section 2.3) is 10^{-19} m^2. This results in a mean free path of order $2 \cdot 10^{-5}$ m, which suggests that the gas cloud is impermeable to the plasma. However, it is important to note that even if it is impermeable to plasma particles, the gas cloud is permeable to the heat flux coming from the plasma. Thus, the gas braking and shock wave generation due to gas heating by the plasma displayed by IMAGINE are likely to be real effects. It is more questionable how strong the frictional braking found in IMAGINE is in reality since this does require gas–plasma interpenetration. By assuming interpenetration, IMAGINE may overestimate this effect. Conclusions from section 4 should therefore be taken with caution.

6. Conclusion and perspectives

The model introduced in this paper is simple in several respects: it uses a 1D radial slab geometry, treats only D_2 MGI into a D^+ plasma, and assumes ionized species to be at rest. Its results are therefore to be taken with caution, keeping in mind the important limitations discussed in section 5. However, the model comprises features which are essential to investigate the fundamental physics of gas penetration during an MGI: the gas equations are based on first principles, and the simulation domain encompasses the plasma, vacuum region and gas reservoir.

In IMAGINE simulations, the gas delivered by MGI is in general strongly braked as it reaches the plasma. This occurs due to two different mechanisms: a gas–plasma friction force and a heating of the gas by the plasma. Both mechanisms are related to charge exchange and recombination. The heating mechanism typically dominates in high temperature, pre-TQ plasmas, whereas the friction mechanism dominates in cold, post-TQ plasmas. The strong gas braking results in a partial penetration of the gas into the plasma and provokes the appearance of a shock wave in the gas, which propagates away from the plasma, braking and compressing the incoming gas. It is important to note that, although the IMAGINE model is presently restricted to D_2 MGI into a D^+ plasma, we expect these mechanisms to generalize to cases where the gas is of a different species than the plasma ions. Implementing other gases than D_2 in MGI is a direction for future work. Another important question for future research is whether the hypothesis of ionized species being at rest is justified or whether the gas may 'push' the plasma in the radial direction.

Simulation results are quantitatively consistent, at least in terms of orders of magnitude, with experimental observations for a D_2 MGI in an Ohmic JET pulse. We stress that no parameter was adjusted in order to match experimental measurements. In fact, the model does not contain adjustable parameters besides the diffusion coefficients D and χ, which only have a small effect on the results. More simulations and comparisons to experiments are necessary to assess whether the model, in spite of its simple geometry, really has a predictive capability or whether the agreement reported in this paper is fortuitous.

IMAGINE allows investigating possible differences between machines regarding experiments aiming at RE beam mitigation with MGI. Simulations show that the gas penetration depth is a decreasing function of the electron density of the target plasma. It may be that at JET, the density of the background plasma co-existing with the RE beam, $n^0_{e,bg}$, is too high for the gas to be able to reach the beam, which would explain its absence of effect. In contrast, in Tore Supra and ASDEX-U, $n^0_{e,bg}$ is one order of magnitude lower and the gas may penetrate, consistently with the positive experimental results. However, in DIII-D, in spite of a value of $n^0_{e,bg}$ comparable to JET, a positive result is obtained. It may be noticed that $T^0_{e,bg}$ is one order of magnitude lower in DIII-D than in JET, but IMAGINE simulations indicate that this should not affect gas penetration much. Further investigations are therefore needed to identify possible origins of the difference between JET and DIII-D.

Another important area for future work is to implement the physics treated in IMAGINE in other models used for MGI simulations, e.g. 3D non-linear MHD codes such as JOREK or NIMROD: the gas deposition model in these codes is indeed rather ad hoc at present, which limits their predictive capability.

Acknowledgments

We would like to thank H. Bufferand, E. Joffrin, B. Pégourié and C. Sommariva for helpful discussions or comments on the manuscript. This work has been carried out within the framework of the EUROfusion Consortium and has received funding from the Euratom research and training programme 2014–2018 under grant agreement No 633053. The views and

opinions expressed herein do not necessarily reflect those of the ITER Organization or the European Commission.

Appendix. Details on simulation settings

In this appendix, we detail how the initial density $n_{\rm res}^{\rm sim}$ and pressure $P_{\rm res}^{\rm sim}$ and of the reservoir and its radial extent $\delta_{r,\rm res}^{\rm sim}$ are set so as to match the initial number of D atoms in the reservoir $N_{\rm res}$, the initial flux of D atoms out of it $\Phi_{\rm res}$, and the initial sound velocity in the reservoir $c_{\rm s,res}$.

One should keep in mind that in the simulations, $n_{\rm n}$ is the D atom density but in reality the gas is made of D_2 molecules. In the equations below, we use a superscript to specify whether quantities refer to D atoms or D_2 molecules.

Considering the simulation domain as a slab of length $2\pi R_0$ and height $2\pi a$, with R_0 the major radius and a the minor radius of the machine, the three abovementioned conditions translate to:

$$N_{\rm res}^{D} = 2V_{\rm res}^{\rm exp} n_{\rm res}^{{\rm exp},D_2} = 4\pi^2 R_0 a \delta_{r,\rm res}^{\rm sim} n_{\rm res}^{{\rm sim},D}, \tag{A.1}$$

$$\Phi_{\rm res}^{D} = 2A_{\rm orifice}^{\rm exp} c_{\rm s,res}^{{\rm exp},D_2} n_{\rm res}^{{\rm exp},D_2} = 4\pi^2 R_0 a c_{\rm s,res}^{{\rm sim},D} n_{\rm res}^{{\rm sim},D}, \tag{A.2}$$

$$c_{\rm s,res}^{{\rm exp},D_2} = \left(\gamma_{D_2} \frac{P_{\rm res}^{{\rm exp},D_2}}{2m_D n_{\rm res}^{{\rm exp},D_2}}\right)^{1/2} = c_{\rm s,res}^{{\rm sim},D} = \left(\gamma_D \frac{P_{\rm res}^{{\rm sim},D}}{m_D n_{\rm res}^{{\rm sim},D}}\right)^{1/2}. \tag{A.3}$$

Equation (A.2) anticipates on the result presented in the next section that the gas velocity at the exit of the DMV is the sound velocity (both in the experiment and simulation).

After some simple algebra, equations (A.1)–(A.3) yield the following expressions for the input parameters $n_{\rm res}^{{\rm sim},D}$, $P_{\rm res}^{{\rm sim},D}$ and $\delta_{r,\rm res}^{\rm sim}$:

$$n_{\rm res}^{{\rm sim},D} = \frac{2A_{\rm orifice}^{\rm exp}}{4\pi^2 R_0 a} n_{\rm res}^{{\rm exp},D_2} = \frac{2A_{\rm orifice}^{\rm exp}}{4\pi^2 R_0 a} \frac{P_{\rm res}^{{\rm exp},D_2}}{k_{\rm B} T_{\rm res}^{{\rm exp},D_2}}, \tag{A.4}$$

$$P_{\rm res}^{{\rm sim},D} = \frac{\gamma_{D_2}}{\gamma_D} \frac{A_{\rm orifice}^{\rm exp}}{4\pi^2 R_0 a} P_{\rm res}^{{\rm exp},D_2}, \tag{A.5}$$

$$\delta_{r,\rm res}^{\rm sim} = \frac{V_{\rm res}^{\rm exp}}{A_{\rm orifice}^{\rm exp}}, \tag{A.6}$$

where $V_{\rm res}^{\rm exp}$ is the volume of the gas reservoir in the experiment.

In JET pulse 86887, the experimental parameters are $P_{\rm res}^{{\rm exp},D_2} = 5$ bar, $T_{\rm res}^{{\rm exp},D_2} \simeq 300$ K, $V_{\rm res}^{\rm exp} = 10^{-3}$ m^3 and $A_{\rm orifice}^{\rm exp} = 7 \cdot 10^{-4}$ m^2 and we use $a = 1$ m and $R_0 = 3$ m. This results in $n_{\rm res}^{{\rm sim},D} = 1.43 \cdot 10^{21}$ m^{-3}, $P_{\rm res}^{{\rm sim},D} = 2.48$ Pa and $\delta_{r,\rm res}^{\rm sim} = 1.43$ m. It may be surprising that the reservoir pressure in the simulation is so low compared to the experimental one (2.48 Pa versus 5 bar). However, it should be kept in mind that in our model the plasma is completely surrounded by the gas reservoir and the incoming gas flow is spread over the whole plasma surface instead of being very localized.

References

[1] Reux C. *et al* 2015 *Nucl. Fusion* **55** 093013
[2] ITER Physics Expert Group on Disruptions, Plasma Control and MHD and ITER Physics Basis Editors 1999 *Nucl. Fusion* **39** 2251
[3] Hender T.C. *et al* 2007 Progress in the ITER Physics Basis chapter 3: MHD stability, operational limits and disruptions *Nucl. Fusion* **47** S128–202
[4] Lehnen M. *et al* 2015 *J. Nucl. Mater.* **463** 39–48
[5] Hollmann E.M. *et al* 2015 *Phys. Plasmas* **22** 021802
[6] Thornton A.J. *et al* 2012 *Nucl. Fusion* **52** 063018
[7] Bozhenkov S.A. *et al* 2008 *Plasma Phys. Control. Fusion* **50** 105007
[8] Reux C. *et al* 2010 *Nucl. Fusion* **50** 095006
[9] Bozhenkov S.A. *et al* 2011 *Nucl. Fusion* **51** 083033
[10] Lehnen M. *et al* 2011 *Nucl. Fusion* **51** 123010
[11] Pautasso G. *et al* 2015 *Nucl. Fusion* **55** 033015
[12] Hollmann E.M. *et al* 2006 DIII-D studies of massive gas injection fast shutdowns for disruption mitigation *Proc. of the 33rd EPS Conf. on Plasma Physics (Rome, 19–23 June 2006)* ECA vol **30I** P-5.136
[13] Leonov V.M. and Zhogolev V.E. 2005 *Plasma Phys. Control. Fusion* **47** 903–18
[14] Fable E. *et al* 2016 *Nucl. Fusion* **56** 026012
[15] Landman I.S. *et al* 2011 *Fusion Eng. Des.* **86** 1616–9
[16] Pestchanyi S. *et al* 2012 *Fusion Eng. Des.* **87** 1195–200
[17] Pautasso G. *et al* 2008 Fusion Energy 2008 *Proc. 22nd Int. Conf. (Geneva, 2008)* (Vienna: IAEA) CD-ROM file [EX/P9-1] and www-naweb.iaea.org/napc/physics/FEC/FEC2008/html/index.htm
[18] Izzo V.A. 2013 *Phys. Plasmas* **20** 056107
[19] Izzo V.A. *et al* 2011 *Nucl. Fusion* **51** 063032
[20] Izzo V.A., Parks P.B. and Lao L.L. 2009 *Plasma Phys. Control. Fusion* **51** 105004
[21] Izzo V.A., Whyte D.G., Granetz R.S., Parks P.B., Hollmann E.M., Lao L.L. and Wesley J.C. 2008 *Phys. Plasmas* **15** 056109
[22] Izzo V.A. 2006 *Nucl. Fusion* **46** 541
[23] Fil A. *et al* 2015 *Phys. Plasmas* **22** 062509
[24] Rozhansky V. *et al* 2006 *Nucl. Fusion* **46** 367
[25] Pégourié B. *et al* 2007 *Nucl. Fusion* **47** 44
[26] Meier E.T. and Shumlak U. 2012 *Phys. Plasmas* **19** 072508
[27] See http://adas.ac.uk for: H.P. Summers, Atomic Data and Analysis Structure User Manual
[28] Landau L.D. and Lifshitz E.M. 1987 *Course of Theoretical Physics* (*Fluid Mechanics* vol 6) 2nd edn (Oxford: Pergamon)
[29] Parks P.B. and Wu W. 2014 *Nucl. Fusion* **54** 023002
[30] Coffey I. 2015 private discussion
[31] Saint-Laurent F. *et al* 2012 *Fusion Sci. Technol.* **64** 711
[32] Hollmann E.M. *et al* 2013 *Nucl. Fusion* **53** 083004
[33] Pautasso G. *et al* 2015 Generation and suppression of runaway electrons in ASDEX Upgrade disruptions *Proc. of the 42nd EPS Conf. on Plasma Physics (Lisbon, 22–26 June 2015)* P-1.134
[34] Romanelli F. *et al* 2015 *Nucl. Fusion* **55** 014001
[35] Nardon E. *et al* 2017 *Plasma Phys. Control. Fusion* **59** 014006